Supplemental information for: Wetting of nanopores probed with pressure

Sanjin Marion,[1] Michal Macha,[1] Sebastian J. Davis,[1] Andrey Chernev,[1] and Aleksandra Radenovic[1,*]

[1] *Laboratory of Nanoscale Biology, Institute of Bioengineering, School of Engineering, EPFL, 1015 Lausanne, Switzerland*

CONTENTS

S1. Devices 1

S2. AC/DC current measurements and analysis 2
Phase sensitive measurements (AC) and DC resistance 2
Pressure and DC/AC data analysis 3

S3. Capacitance of supported membranes during wetting 5

S4. Finite element model of the nanopore with obstructing objects 6

S5. Wetting artifacts in hydrophilic pores supplemental information 9

S6. Wetting artifacts with 2D materials supplemental information 12

References 17

S1. DEVICES

Supporting membrane fabrication Wafer processing was subdivided into two major technological steps: a) backside photolithography and etching b) frontside e-beam lithography and etching. The process was performed on the wafers from the same batch (supplier Active Business Company), representing 380 microns thick 100 mm intrinsic Si wafer (100) with 60 nm of SiO2, and 20 nm low stress SiN on each side. Throughout the first step during the backside photolithography and dry etching apertures for supporting SiN membranes and dicing lines were formed. Next, wet etching through the wafer thickness was done to physically form the supporting SiN membranes and dicing lines. The second technological step was focused on formation of the low-dimensional front side apertures in 20 nm-thick SiN membranes for the suspension of the 2D material[1]. For that purpose, e-beam lithography was done using 495A4 PMMA as positive resist at 100 kV. The pattern alignment was done using the wet-etched markers that were formed on the 1st step. The exposed pattern was then transferred to the substrate using a dry etching process in CHF3/O2 atmosphere. E-beam resist was then stripped with a microwave plasma stripper following an acid piranha solution cleaning. To finalize preparation, wafer was rinsed with mili-Q water.

Samples used in this study In-house made chips S1 and S2 were produced according to the procedure described above. Different batch runs and membranes had supported membrane sizes ranging from 10×10 to 40×40 μm^2. Two membranes with sample names S3 and S4 were bought from NORCADA (P/N NXPR5001.2Y-75nm-AO/O-HR, L03127-07, supported membrane size 12×12 ($\pm 5\mu$) μm^2, Silicon Nitride of 20nm$\pm$5nm thickness). Samples were cleaned before use with 5 min of O_2 plasma exposure and then filled with liquid previously degassed in a Schlenk flask. HMDS coated samples were primed on ATMsse hotplate system at 125°C using standard photolithographic process, and were not cleaned prior to use. For samples where MoS_2 was transferred (sample codes $S_{MoS_2}1$ to $S_{MoS_2}5$), no cleaning was done before measurement.

* aleksandra.radenovic@epfl.ch

S2. AC/DC CURRENT MEASUREMENTS AND ANALYSIS

Phase sensitive measurements (AC) and DC resistance

When performing phase sensitive measurements with the lock-in we use an external driving potential (probe) of the form

$$V(t) = V_0 \sin \omega t \tag{S1}$$

where $\omega = 2\pi f$ with f the frequency of the sine wave. We then measure a response of the form

$$I(t) = I_1 \sin(\omega t + \phi_1) + I_2 \sin(2\omega t + \phi_2) \tag{S2}$$

where the values I_1 and ϕ_1 correspond to the linear (1st harmonic) response and I_2 and ϕ_2 the first correction due to the nonlinear response in the system (2nd harmonic).

The response of the system to our driving voltage $V(t)$ is characterize by the complex valued admittance $Y(\omega, V_0)$ such that

$$I = Y(V)V$$

any non-linearity in the response of the system is in the admittance. We find that at sufficiently low driving voltages and low frequencies, we see no contributions from any non-linearity in capacitance. For small bias voltages ($\ll 1$ V_{rms}) we assume that any non-linearity is found in the conductance $G(V)$:

$$Y(V) = G(V) + j\omega C.$$

At sufficiently low frequencies (below ~ 100 Hz) the capacity C will be dominated by the capacitance of the supporting membrane[2,3].

The simplest model for the conductivity would be to take a Taylor expansion for small voltage perturbations which is valid for a purely AC external electric field:

$$G(V) \approx G_0 + G_1 V \tag{S3}$$

with $G(V = 0) = G_0$ and $G_1 = \left(\frac{\partial G(V)}{\partial V}\right)_{V=0}$. Typically $G_1 = 0$ due to time and spatial inversion symmetry, but in the case of nanopores it is known that there can be a break in the symmetry due to ionic current rectification[4]. Previous studies on nanopores[5] clearly show that the small biasing voltage response is linear and governed by an equation of the form:

$$G_0 = \kappa\sigma$$

with σ the solution conductivity and κ the geometrical factor

$$\kappa^{-1} = \frac{4L}{\pi d^2} + \frac{1}{d}.$$

In contrast to regular impedance spectroscopy where κ corresponds to a cell shape constant, our sample resistance is dominated by the nanopore opening so that κ is the pore shape constant. The dependence of the resistance R of a MoS_2 nanopore on its diameter d is shown on Fig. S1, with the largest contribution arising from the access region:

Using the nonlinear conductivity model eq. (S3) once can obtain a response to the applied sinisoidal voltage by eq. (S1)

$$I = \frac{1}{2}V_0^2 + (G_0 V_0)\sin(\omega t) + \omega C \cos(\omega t) + \frac{1}{2}G_1 V_0^2 \sin(2\omega t - \frac{\pi}{2})$$

from which we can connect the values measured with the phase sensitive detector eq. (S2) to the phenomenological conductance terms:

$$I_1 \approx G_0 V_0 \sqrt{1 + \frac{\omega^2 C^2}{G_0^2 V_0^2}} \qquad \phi_1 = \tan^{-1}\left(\frac{\omega C}{G_0 V}\right)$$

$$I_2 = \frac{1}{2}V_0^2 G_1 \qquad \phi_2 = -\frac{\pi}{2}$$

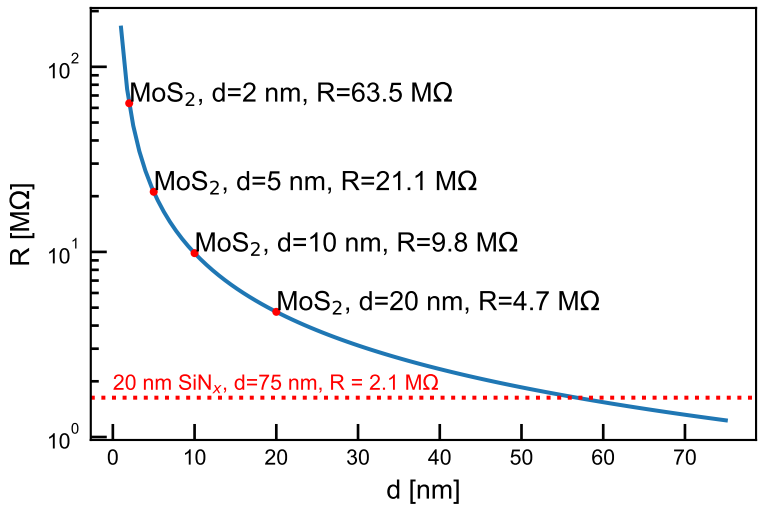

FIG. S1: **Dependence of a MoS_2 nanopore resistance R versus diameter d.** MoS_2 is taken to have a thicknes $L = 0.615$ nm. The solution conductivity is taken to be 110 mS/cm.

and calculate the conversion formulas for capacitance C and resistance R_{ac}:

$$R_{ac} = \frac{V_0}{I_1 \cos\phi}$$
$$C = \frac{I_1 \sin\phi}{\omega}$$

An approximation to the current rectification $r(V) = |I(+V)|/|I(-V)|$ at a DC voltage V can be obtained trough the higher harmonics of the lock-in signal. Taking into account that the linear conductivity is dominant $G_0 \gg G_1 V$ and that we measure at low (DC-like) frequencies $\omega \ll \frac{G_0 V_0}{C}$:

$$r(V) = \left|\frac{I(+V)}{I(-V)}\right| \approx \frac{G_0 + G_1 V}{G_0 - G_1 V} \approx \frac{I_1 + 2I_2}{I_1 - 2I_2}. \tag{S4}$$

Note that a rectification value obtained from an AC signal, will be according to this definition always $r \geq 1$ so that information about the directionality of the rectification is lost.

As proof that our resistance obtained with AC bias R_{ac} is the same as the DC obtained R we provide control measurements on two different pores ($d \sim$ 75,130 nm) in 20 nm silicon nitride. The IV curves provide the same resistance values as the ones obtained from the AC measurement at frequencies below 10 Hz (Fig. S2).

Pressure and DC/AC data analysis

To obtain a relation between a measured value (I, R_{ac}, C, r) versus pressure P we apply the pressure and once it has settled to within 5% of the target pressure value we wait for at least 1 second for DC current measurments I or 2.5 seconds plus 15 times the settling time base of the lock-in (300 ms - 1 s). Using a CUSUM alghoritm implemented in python we identify current segments corresponding to a pressure state. These current segments are then cut so that about the first 70% (to account for settling artifacts) and the last 10% of the segment (to account for synchronisation issues between the lock-in and the pressure system) is excluded. A mean of this signal trace is then used as the representative value at that pressure. This same algorithm is used to extract the noise power spectral densities and the current probability densities (violin plots) from time traces of the current versus applied voltage. In this case, the time trace used for the analysis is at least several seconds long. An example time trace of the measured quantities is provided on Fig. S5.

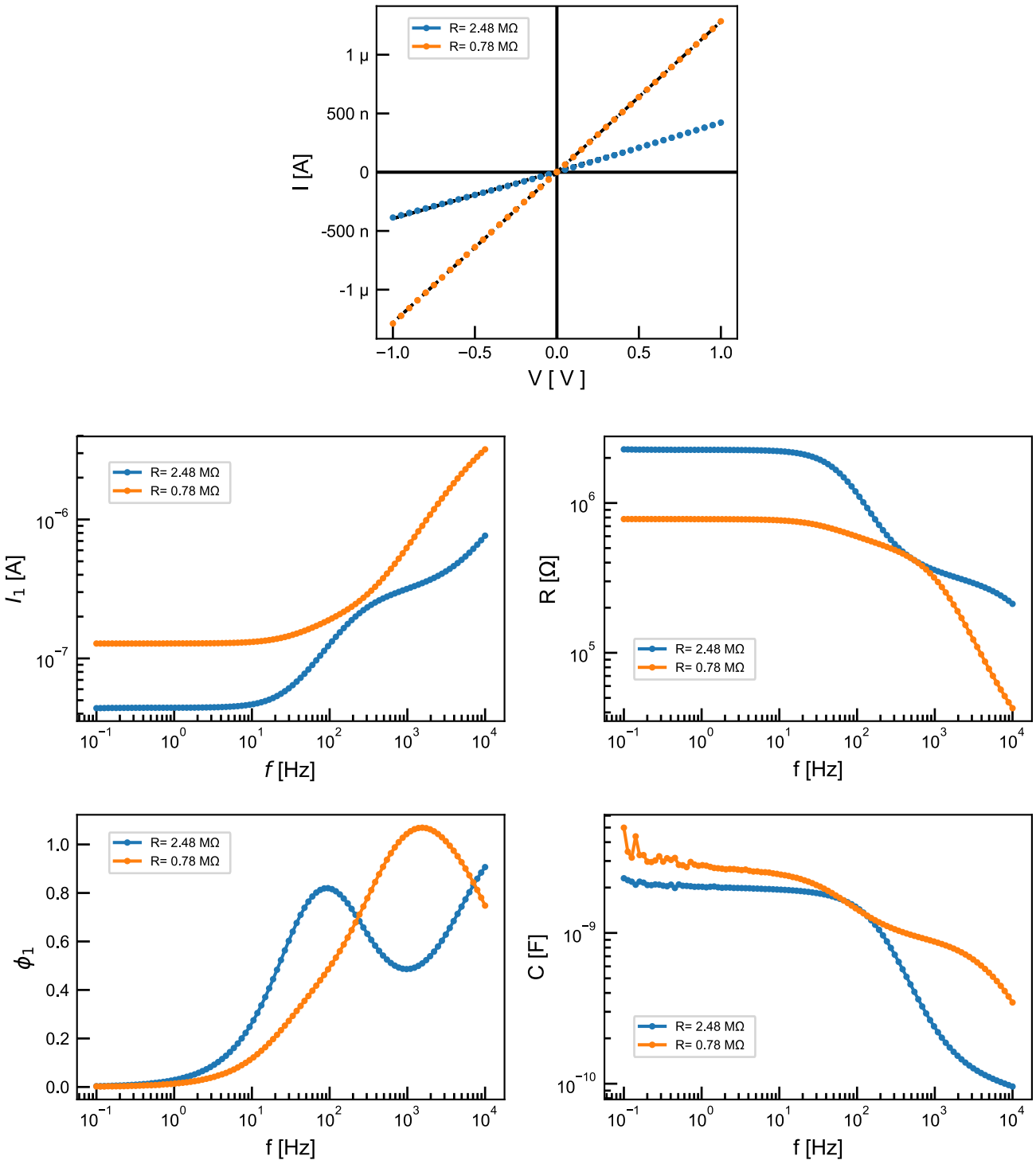

FIG. S2: **Comparison of DC IV curve and AC measurements on two samples.** One sample had a pore size of 130 nm (resistance $R = 0.78$ MΩ), while the other had a pore size of 80nm but was partially cloged or not completely wetted (resistance $R = 2.48$ MΩ). For the AC response the measured current I_1 and phase ϕ_1 as well as the calculated capacitance C and R_{ac} versus input voltage frequency f are provided. All measurements are done with $V_0 = 0.1$ V_{rms}

S3. CAPACITANCE OF SUPPORTED MEMBRANES DURING WETTING

Our aim is to describe how the wetting of the silicon nitride membrane influences its capacitance. The dominant contribution to the chip capacitance obtained trough measurements at low AC frequencies comes from a series connection of the double layer capacitance of the silicon nitride membrane and the capacitance of the membrane itself.[2] Neglecting the contribution of the high resistances, the capacitance C of such a membrane immersed in a salt solution can be approximated as an integral over the whole surface with each small area dA contributing via its local capacitance per unit area $\tilde{C}$

$$C \approx \iint \tilde{C} dA \tag{S5}$$

where $\tilde{C}$ consists then of a series connection of the silicon nitride membrane $\tilde{C}_m$ and the two electrical double layer contributions $\tilde{C}_{dl}$:

$$\frac{1}{\tilde{C}} = \frac{1}{\tilde{C}_m} + \frac{2}{\tilde{C}_{dl}}. \tag{S6}$$

The total local capacitance contribution then will be limited by the lowest capacitance in the series, which is in this case the membrane capacitance.[2]

Let us first discuss the influence of bad wetting on the membrane capacitance $\tilde{C}_m$. The membrane capacitance can be approximated by a parallel plate capacitor $\tilde{C}_m = \epsilon_0 \epsilon_r / d$ with a separation d and a medium of relative permittivity $\epsilon_r \approx 7.5$ for silicon nitride. If a gas bubble covers a surface of area ΔA, then the local capacitance value will be suppressed by the increase in $1/d$ from the added layer of gas, and from the reduction in the local permittivity to a value of $\epsilon_r \approx 1$. We see that already based on this simple argument, the total local capacitance $\tilde{C}$ will be reduced by at least one order of magnitude just based on this scaling argument as it is limited by the reduction of $\tilde{C}_m$. In that sense, in the first order of approximation a surface air bubble will reduce the contribution to the capacitance proportional to its surface area ΔA. A more detailed analysis would require knowledge of the exact nature and shape of the bubble.

The double layer contribution to the capacitance is proportional to the surface area of the interface between the electrolyte and another medium. Let us take a simple example in which a membrane of surface area A, immersed in a salt solution, has a bubble on one of its surfaces. We will simplify by assuming that the bubble shape is approximated as a spherical cap of radius r, so that the unwetted surface area of the membrane is $a = \pi r^2$. The new surface of the membrane capacitor is now defined by the shape of the bubble on one side, and the membrane surface on the other side. Thus, a spherical bubble will increase the total area of the double layer, but the question is how will the double layer capacitance depend on the effective surface charge and nature of the gas-liquid interface.

To give some insight on the double layer capacitance, we can use a simple model for its differential capacitance. The double layer differential capacitance $\tilde{C}_{dl}$ can be modeled as a series connection of a diffuse layer part $\tilde{C}_d$ and a compact layer part $\tilde{C}_c$,[6] such that:

$$\frac{1}{\tilde{C}_{dl}} = \frac{1}{\tilde{C}_d} + \frac{1}{\tilde{C}_c} \tag{S7}$$

For the diffuse layer capacitance a good model for dilute salt solutions is the Gouy-Chapman theory which gives[6]

$$\tilde{C}_d = \frac{\epsilon_0 \epsilon_r}{4\pi\lambda_D} \cosh\left(\frac{e\phi}{2k_B T}\right) \tag{S8}$$

with ϕ the potential drop across the double layer, λ_D the Debye length and $k_B T/e \approx 25.7$ mV. The compact layer capacitance can then be approximated as $\tilde{C}_c = \frac{\epsilon_0 \epsilon_{eff}}{4\pi\delta}$ with delta the distance of closest approach of the ions to the surface and ϵ_{eff} an effective relative permittivity. Importantly, the capacitance depends on the potential drop ϕ, which is directly dependent on the surface charge density at the air-liquid or solid-liquid interface, and will be higher for highly charged surfaces. In our case we know that the surface charge of bubbles with diameters in the micron range[7] is expected to be below the values for the silicon-nitride interface[8] at the salt and pH conditions we use. We note that this is not necessarily true for nanobubbles[9], so that for example surface patterned with hydrophobic patches could depending on the conditions lead to an increase in the total capacitance in respect to a membrane not covered with any bubbles. Still, even if the double layer capacitance is increased, it will be limited by the reduction in the membrane capacitance part in the presented model. In our case, we see in Fig. 1c,d that the capacitance increases during bubble absorption, and in no case did we notice that after applying degassed solutions and under compression pressure did the capacitance of the membrane start decreasing after a successful first wetting of the membrane.

S4. FINITE ELEMENT MODEL OF THE NANOPORE WITH OBSTRUCTING OBJECTS

A finite element method was implemented on an axially symmetric system in COMSOL multiphysics (version 5.5). The system was modeled as in[10,11] by coupled Poisson-Nernst-Planck-Stokes equations. Electrostatic interactions between bound (surface charge on the silicon nitride-water and gas-water interfae) and free charges (added salt) were modelled using the Poisson equation for the electrostatic potential $\phi(\mathbf{r})$

$$\nabla^2\phi(\mathbf{r}) = -\frac{\rho(\mathbf{r})}{\epsilon_0\epsilon_r} \tag{S9}$$

with $\rho(\mathbf{r}) = eN_a\sum_i z_i c_i(\mathbf{r})$ the density of free charge carriers with z_i the valency and c_i the density in mol/m^3 of the ion i, and ϵ_r the relative permitivity of the material (80 for water, 7.7 for silicon nitride, 1 for air). Here the free charge densities c_i were subject to the Nerst-Planck equations for the ion flux $\mathbf{J}_i$ of species i with convection due to fluid flow with a velocity $\mathbf{u}(\mathbf{r})$:

$$\mathbf{J}_i = -D_i\nabla c_i - \frac{D_i}{k_BT}z_i e c_i\nabla\phi(\mathbf{r}) + c_i\mathbf{u}(\mathbf{r}) \tag{S10}$$

where D_i are the diffusion constants for the ions ($D_1 = D_2 = 2\cdot 10^{-9}\ m^2/s$).

Fluid flow was obtained using the Stokes equation with an electric body force $\rho(\mathbf{r})\nabla\phi(\mathbf{r})$ and pressure gradient ∇p:

$$\eta\nabla^2\mathbf{u} = \rho(\mathbf{r})\nabla\phi(\mathbf{r}) + \nabla p \tag{S11}$$

with η the dynamic viscosity of water using the built in COMSOL parameters.

The FEM mesh was constructed in COMSOL similar to previous works[10–12] using boundary layer refinement with minimal size at boundaries of $0.1nm$ and growth ratio of 1.2. Near all corners and at the nanopore oppening the mesh was additionally refined until convergence was obtained. First a 1D problem on the boundary of the simulation domain was solved without fluid flow and then used as the boundary condition for the full problem[10], with pressure applied on all the external boundaries on both sides of the chamber.

We studied four possible cases of nanopores representing: a) an open pore (Fig. S3a), a pore with an obstruction (bubble) sitting at the pore edge on one side of the chamber (Fig. S3b), a pore with a circular obstruction (clog) (Fig. S3c) and a pore with a spherical unwetted part constricting the pore (Fig. S3d). In all cases the supported silicon nitride membrane was taken to be 20 nm thick with a nanopore diameter of $d = 40$ nm. The air bubble was taken to have a radius of $r_b = 80$ nm and the electrolyte concentration to be $c = 1$ M. The surface charge at the solid-liquid interface (silicon nitride to water) was taken to be $\sigma_{ls} = -50$ mC/m^2 and the charge at the gas-liquid interface (air bubble to water) was taken to be $\sigma_{gs} = -20$ mC/m^2, in accordance with zeta potential measurements on silicon nitride pores[8] and microbubbles[7]. We note that a larger surface charge in the case of the air-gas liquid interface would only enhances ionic current rectification. Details about each simulation geometry are provided in the figure caption.

In order to probe for how the four static cases of obstructions at the nanopore influence the conductance, we extract the total current going trough the system at different bias voltages (from -300 mV to 300 mV) and under different pressure gradients ($P = 0, \pm 5$ bar). Fig. S4a shows the current versus voltage curves (IV) for an open pore compared to the bubble case. An open pore is seen to have zero ionic current rectification ($r = 1$) under no pressure, and a small level of ionic current rectification under a pressure gradient which comes from the convective contribution to the ion transport ($r < 1.005$). In comparison, in the same geometry but with a bubble present on the side we see that there is a measurable ionic current rectification ($r = 1.014$) which is reduced under pressure gradient. This effect has already been well documented in the literature[13,14], and is explained as coming from the fluid flow destroying the concentration polarization effect inside the pore arising from the asymmetry of the nanopore and the presence of surface charges. In the case of a clog particle (Fig. S4a) we see that the pressure gradient is not sufficient to reduce the ionic current rectification completely from its zero pressure value ($r = 0.97$) but it modulates the value. This is also in accordance with known results that if the rectifying nanopore is too small, the fluid flow rate is not sufficient to nullifying the ionic current rectifying effect of the concentration polarization.[13] In this case, conduction is proceeding through a thin ring formed at the point of closest separation which due to access effects limits the total fluid flow. Lastly, we find that in the case of a symmetrical unwetted pore (Fig. S4c) we have no ionic current rectification ($r = 1$). In all three cases, the resistance of the nanopore is increased by the presence of the obstruction, but the conductance stays linear in respect to the applied voltage.

We conclude that neither of the static models presented here can account for the large change in ionic rectification and resistance, as seen in the main text, but that a dynamic model is required. We suggest that the most likely scenario is that due to improper wetting, a nanobubble is moved around the entrance and deformed by the pressure driven fluid flow.

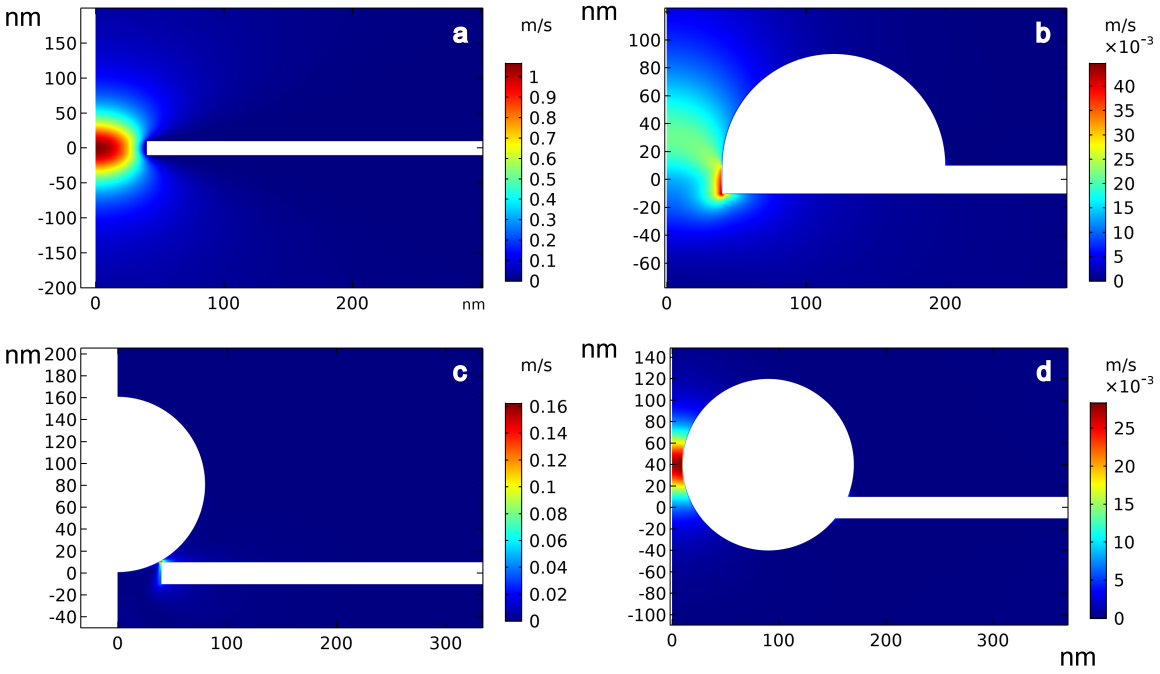

FIG. S3: **FEM model demonstrating magnitude of the electroosmotic flow velocity**. Surface profiles are provided for the case of an applied potential difference of 300 mV. The system has axial symmetry around the center of the nanopore. Panels show: a) unobstructed nanopore (open pore case), b) an air bubble on one side of the nanopore (bubble case, note that due to the axial symmetry the surface nanobubble is actually "doughnut"-shaped), c) an object (air) obstructing the entrance of the nanopore (clog case). Here a gaseous obstruction was placed at the pore opening, almost completely obstructing it. The distance of closes seperation betwen the spherical obstruction and the silicon nitride membrane was chosen to be$\approx$ 4 nm so as to enable easy convergence at the double layer region on the boundaries. d) nanopore entrance obstructed by a symmetrical air bubble (unwetted case). A gaseous obstruction was placed at the pore opening so that it is constricting the pore size. The resulting radius of the opening was chosen to be 10 nm in radius, with the center of the gas obstruction shifted by 40 nm from the center of the simulation box.

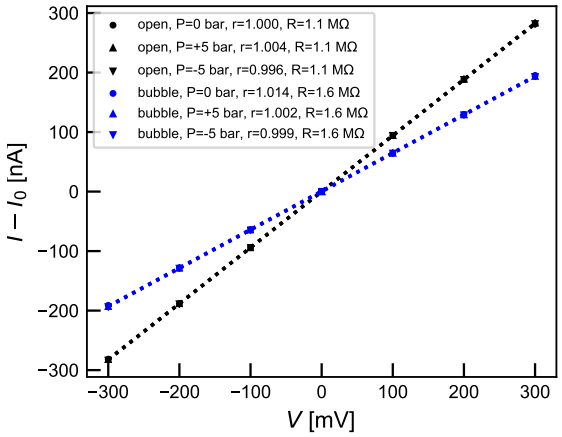

(a) Comparison between open pore (Fig. S3a) and the bubble case (Fig. S3b).

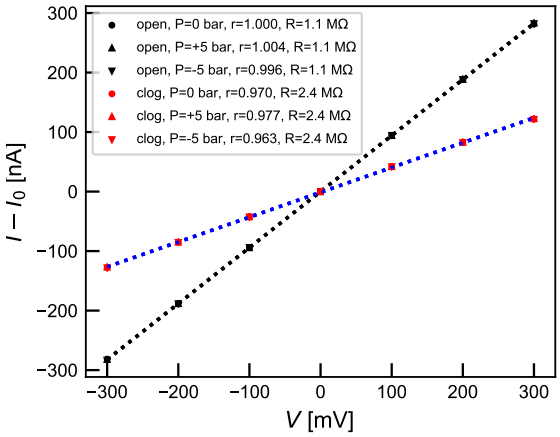

(b) Comparison between open pore (Fig. S3a) and clog case(Fig. S3c).

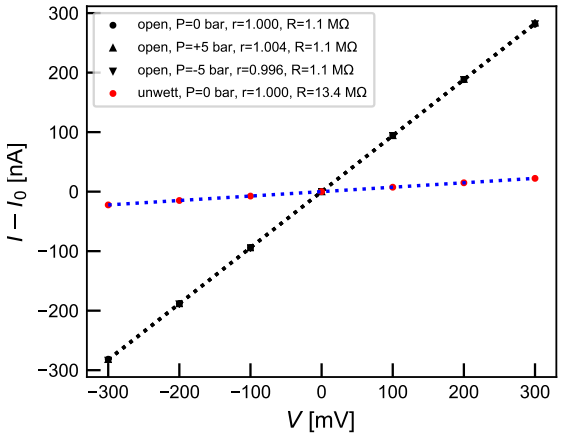

(c) Comparison between open pore (Fig. S3a) and the unwetted case(Fig. S3c).

FIG. S4: **Current versus voltage curves extracted from the FEM models representing the open nanopore case (Fig. S3a), bubble case (Fig. S3b), clogged case (Fig. S3c), and unwetted case (Fig. S3d).** Figure legend note the level of applied pressure gradient (P), and the resutling ionic current rectification (r) and pore resistance (R).

S5. WETTING ARTIFACTS IN HYDROPHILIC PORES SUPPLEMENTAL INFORMATION

Sample S1: We provide the full time trace of the measured AC data for Fig. 3c (Fig. S5. Fig. S6 shows the current time trace and the plot of the flicker noise amplitude dependence on current for Fig. 3c. Sample was filled with incompletely degassed solution by pipetting from Schlenk flasks into syringes.

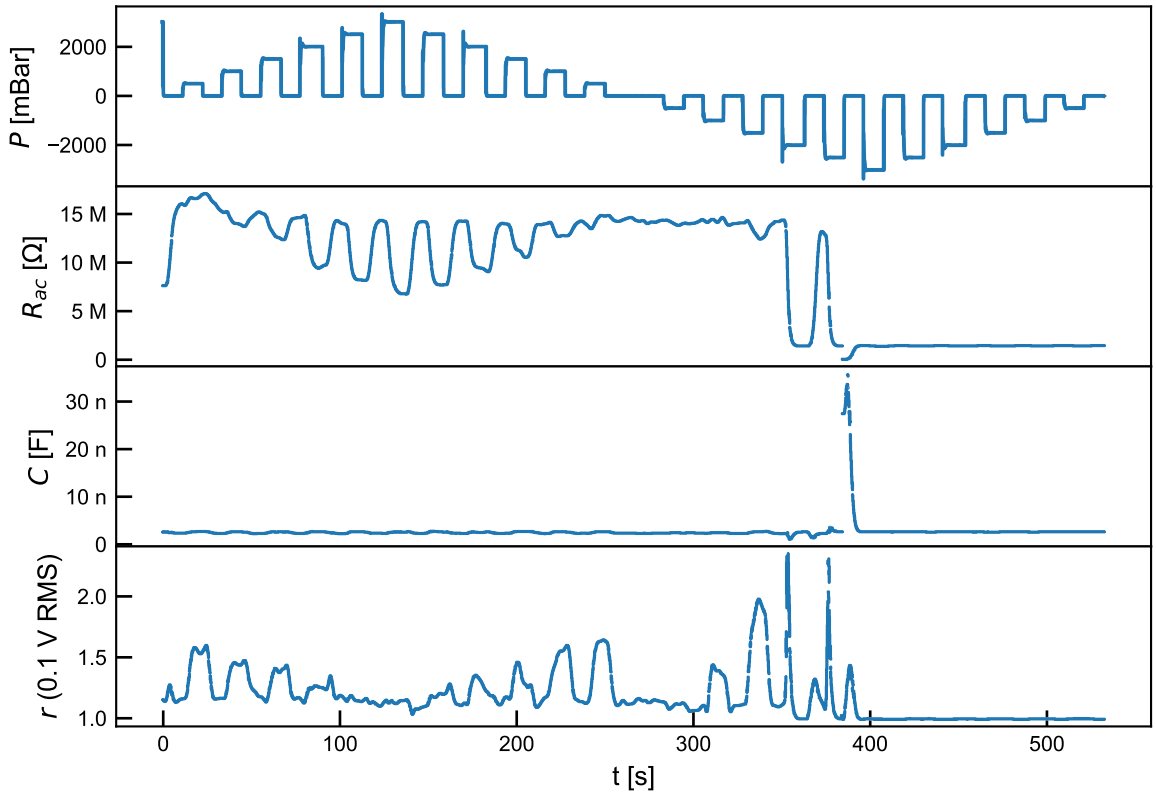

FIG. S5: **Sample S1: Time trace for Fig. 3c in the main text.** Raw time trace of the applied pressure and the measured R_{ac}, C and r.

Sample S2: Sample was filled with incompletely degassed solution by pipetting from Schlenk flasks into syringes. After filling the sample presented similar behaviour as in Fig. 3 of the main text. Fig. S7a shows how the system IV curve changed from a linear ($\Delta P = 0$) to a nonlinear IV curve under the application of pressure ($\Delta P \pm 3$ bar), ending in a partially closed state at the end ($\Delta P = 0$). The power spectral density (Fig. S7b) indicates an increase in noise during this process, with the lowest noise in the open starting state, followed by the ending partially clogged state, with the both states under pressure expressing a higher level of Flicker noise. A pressure sweep (Fig. S7c,d) shows that the same direction which caused the unwetting of the pore is also increasing both the resistance R_{AC} and ionic current rectification r as measured with an AC stimuli, with the state at $P = 0$ indicating good wetting.

Sample S3: Sample was filled with incompletely degassed solution by pipetting from Schlenk flasks into syringes. After filling the sample picked up a bubble/obstruction under pressure (Fig. S7e) which resembles the same profile as in Fig. 3c but with a higher resistance value. IV curves performed after this indicate that the nanopore is not completely wetted and that the noise level is highest when a pressure gradient of the opposite direction than the one which caused a bubble pick-up is applied. After flushing with freshly degassed solution and applying compression pressure for several minutes the nanopore IV curve linearized. As the chip was reused, we can not confirm that the chip hasn't at least partially clogged.

Sample S4: Sample was filled with incompletely degassed solution by pipetting from a Schlenk flask into a syringe. Sample was filled using compression pressure, after which an application of a pressure gradient reduced the resistance

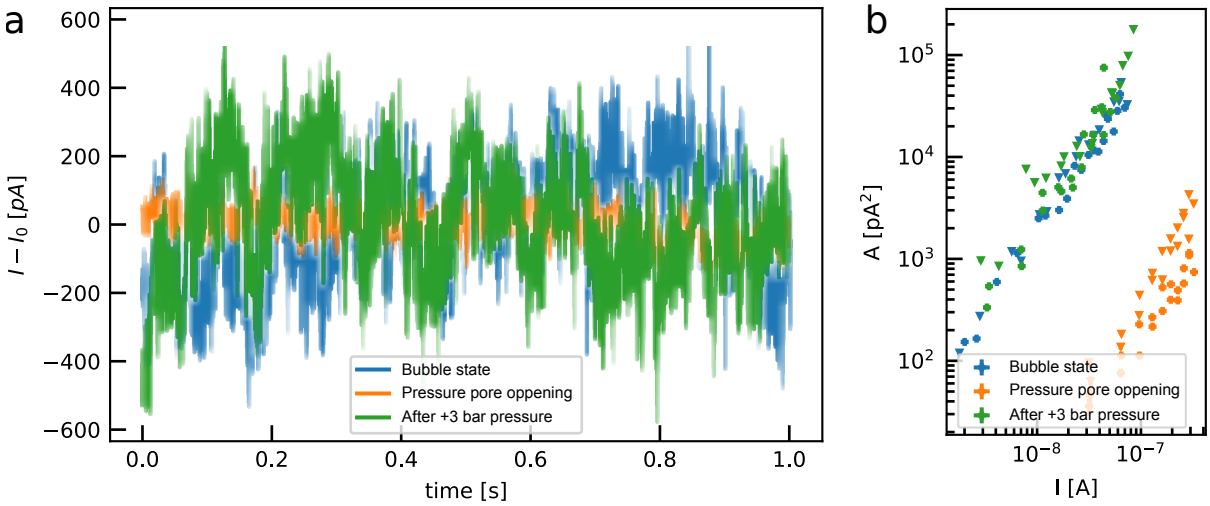

FIG. S6: **Sample S1: Current traces and noise scaling.** a) Current traces versus time used to obtain the points at 0.5 V and the corresponding PSD in the main text Fig. 3a,b. b) The flicker amplitude A versus the current magnitude I through the nanopore obtained from a fit of the form A/f to the PSDs for Fig. 3a for different driving voltages. Triangles denote I values at negative currents, crosses at positive currents.

(Fig. S7f). This was followed with an increase in noise, as expected for bad wetting.

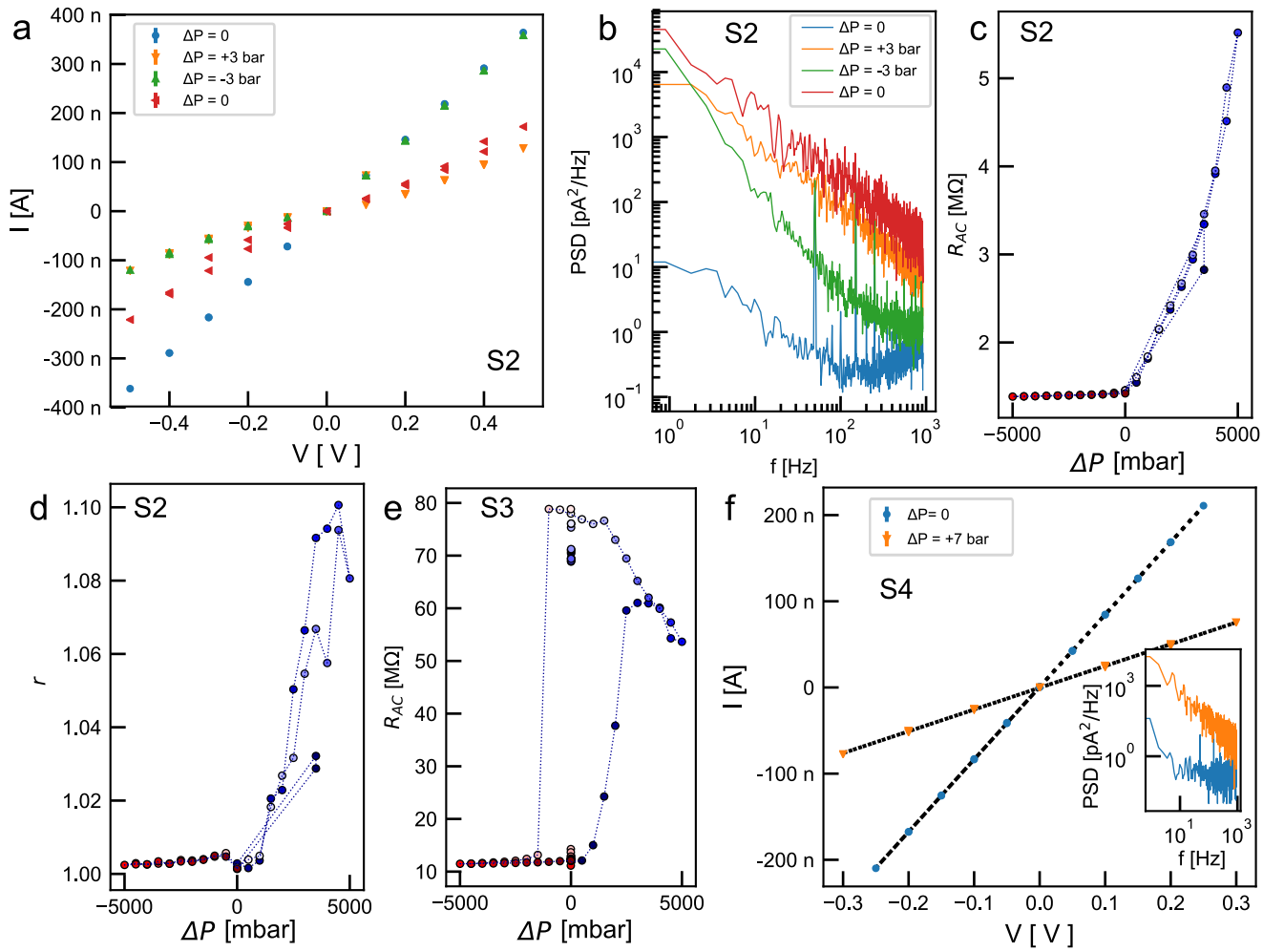

FIG. S7: **Wetting artifacts in hydrophilic pores** a) Example of pressure switching of a bubble in for sample S2. An IV curve is provided for four subsequent measurements done under an applied pressure of $\Delta P = 0, 3, -3, 0$ bar. b) Current power spectral density obtained from the first point in the IV curve from panel a at 0.2 V. Note that the open pore is moved into a closed state with positive pressure. A negative pressure partially recovers the open state with a lower noise than with positive pressure, but higher than in the original open state, and with strong ionic current rectification. After this the pore is still in a closed state but with a lower noise level than when either the positive or negative pressure was applied. c) Pressure switching of the bubble measured 2h after panel b. d) Ionic current rectification measured simultaneously as data on panel c. e) Example of a pressure switching of a bubble inside the nanopore. The sample returns to a higher value of 10 MΩ as it was reused and cleaned in Piranha for 2h after being immersed in salt previously. This might have increased the hydrophobicity of the pore, but also could have cause clogging artifacts to be present. f) Example of bubble pick-up due to pressure. The first IV curve is recorded immediately after filling (linear fit to a resistance of $R = 1.12$ MΩ), and the second one is recorder under a pressure of $\Delta P = 7$ bar (linear fit to a resistance of $R = 4.0$ MΩ). The inset shows the noise power spectral density for the two IV curves showing how the noise is considerably increaced in the obstructed case.

S6. WETTING ARTIFACTS WITH 2D MATERIALS SUPPLEMENTAL INFORMATION

Sample $S_{MoS_2}1$: The sample was imaged in TEM and drilled to have several pore of several nanometers in diameter (Fig. S8a). The pore was filled with degassed 1M KCl buffered at pH8 as described in the main text. After the application of 7 bar compression pressure for several minutes it demonstrated a fluctuating nonlinear IV curve (Fig. S8b) which relaxed in time to a higher resistance and noise level matching the trends shown in the first IV curve (Fig. S8c). After about 12h of wait, the system exhibited a stable and more conductive nonlinear IV curve (Fig. 4a in the main text), which was then linearized with compression pressure and flushing with fresh degassed solutions (Fig. 4b). After that a solvent exchange with ethanol was performed which increased the resistance. Application of a pressure gradient in this state indicated that there were further wetting issues.

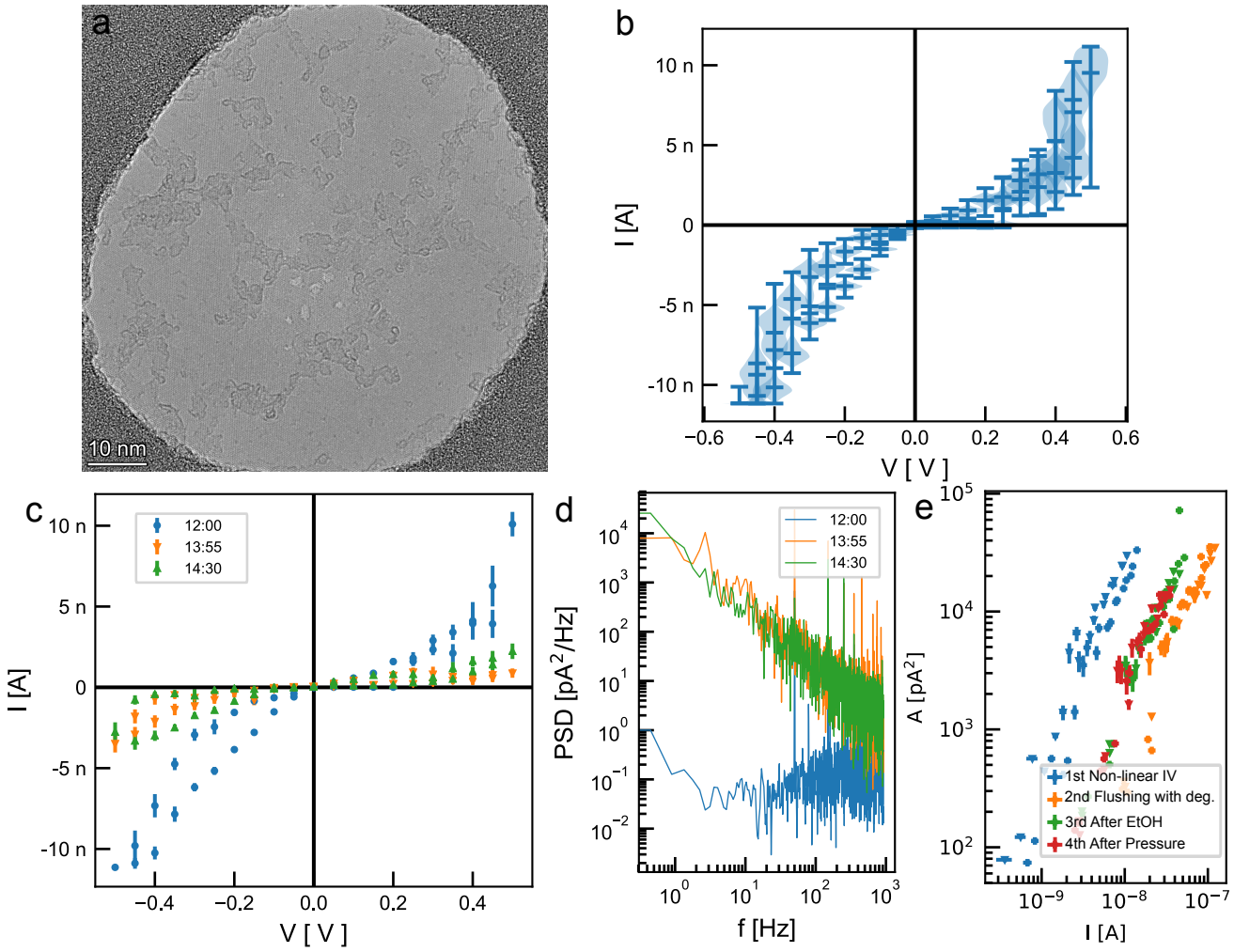

FIG. S8: **Sample $S_{MoS_2}1$**: a) Transmission electron microscope images of MoS_2 sample before measurements. Imaged with FEI TEM Talos at 80 kV in HRTEM mode. Visible nanopores were drilled by beam condensation with in-situ control of the pore formation. b) Immediately after filling and a day before the measurements in Fig. 4a,b of the main text. The bars denote extrema of the current probability density distributions, while the shapes denote the probability density for finding the current at that value (violin plot). The amplifier range was limited to measuring ±10 nA. c) Time evolution of the IV curve from panel b. During this time the IV curve was let to settle with no disturbances. Further applications of pressure in the range of ±3 bar did not change the IV curve shape. If one were to extrapolate the resistance of these pores in the ±0.2 V range one would obtain resistances (and effective MoS_2 diameters) of 140 MΩ (1.1 nm) and for the last two curves 500 MΩ (0.5 nm). Yet, from TEM images we expect a nanopore in the several nm size range. d) The noise poser spectral density for the data presented on panel c (at 0.2 V) increased considerably during the time that the apparent resistance also increased and fluctuations of the current reduced. Note that the amplifier noise in this current range is about 20 fA/$\sqrt{\text{Hz}}$. e) Supporting figure for main text figures 4a,b inset showing the scaling of the flicker noise amplitude A versus the magnitude of the current I obtained from a fit to an equation of the form A/f for the noise PSD for different driving voltages. Triangles denote I values at negative currents, crosses at positive currents.

Sample $S_{MoS_2}2$: The sample was put in a 1:1 ethanol and de-ionized water for 20 minutes, before being placed into the chamber and filled with 1M KCl solution buffered at pH 8 (as described in the Methods section of the main text). After filling, the system was found to be switchable between two states (Fig. 4c,d,e and Fig. S9a as described in the main text. A measurement of the DC under applied voltage during a pressure sweep is provided (Fig. S9b matching the AC measurements. Two two streaming curves (streaming potential V_s versus pressure P) obtained with the sample before and after the data shown on Fig. 4c in the main text are also shown on Fig. S9c. We used streaming potential as it does not have a specific dependence on the resistance of the sample, as in the case of streaming current which is more commonly used. The streaming potential is related to the zeta potential ζ of the surface and the applied pressure gradient ΔP as $V_s = \epsilon_r \epsilon_0 \zeta \Delta P / \eta \sigma$ in the regime of high salt concentrations when surface conduction effects can be neglected, with η the dynamic viscosity of the fluid and σ the bulk conductivity of the sample. Measurements were obtained with a home-made electrometer buffer amplifier with a > 1 TΩ input impedance. Here, the zeta potentials obtained before and after. We find that stable streaming potential is an indicator of an open fluidic pathway between two sides of the membrane. But, a thus obtained zeta potential value will highly depend on the pore size and the geometry,[15] so we can not infer the correct value of the zeta potential and correlate it with different states of the sample.

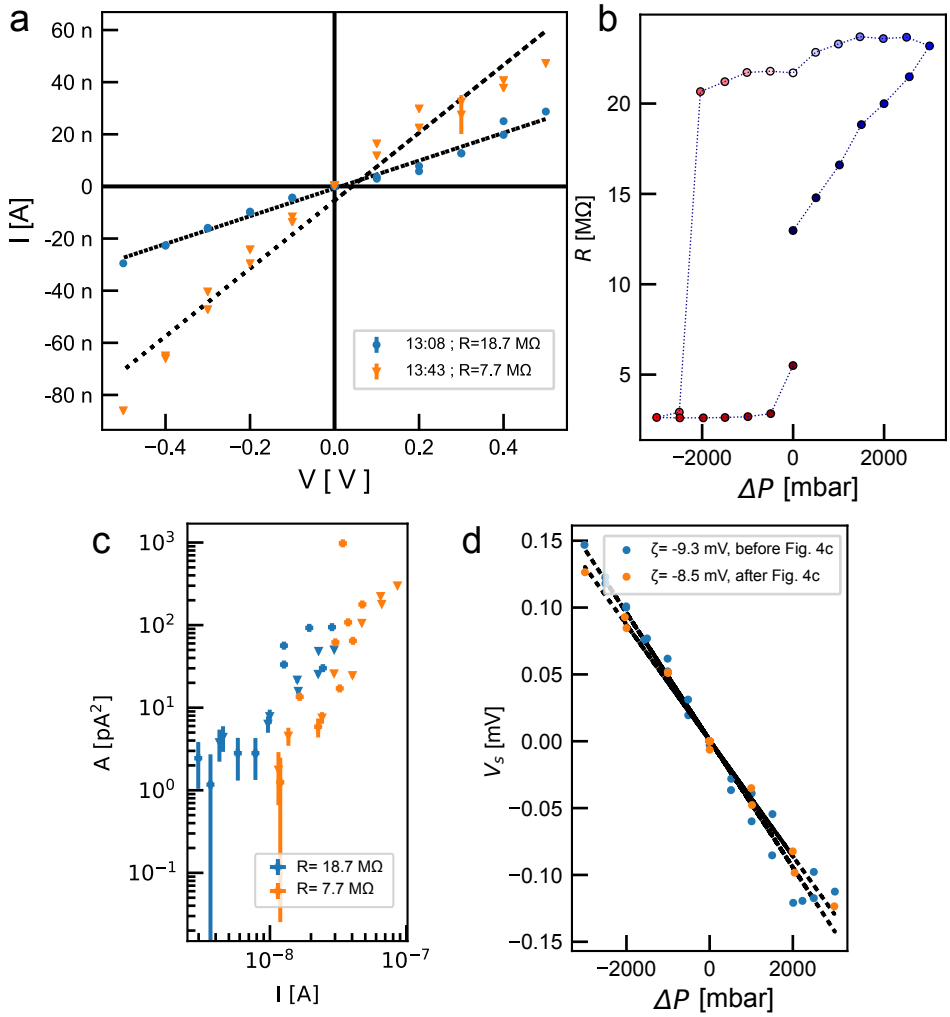

FIG. S9: **Sample $S_{MoS_2}2$**: a) IV curves from which the current power spectral density in Fig. 4e of the main text was obtained. b) DC pressure sweep done after the Fig. 4c,d in the main text. This curve confirms that the switching behavior seen in the AC measurement is not an artifact of using AC current for the measurement. The curve is obtained at a 0.1 V DC bias. c) A plot of the flicker noise amplitude A scaling versus current amplitude I obtained from a fit of $A/f + B + Cf$ to the noise PSD shown in Fig. 4e in the main text for different driving voltages (panel a). Here due to low noise in the high resistive state a model including both the shot and dielectric noise was used. Triangles denote I values at negative currents, crosses at positive currents. d) Streaming potential V_s curves performed before and after Fig. 4c in the main text.

Sample $S_{MoS_2}3$: The sample was TEM imaged and no pores were found (Fig. S10a). After that the sample was put in a 1:1 ethanol and de-ionized water for 20 minutes, before being placed into the chamber and filled with 1M KCl solution buffered at pH 8 (as described in the Methods section of the main text). We found that the system filled under compression pressure, indicating an nonlinear IV curve which was consistent with the application of gradient pressures (Fig. S10b,c) with a high level of noise present and instabilities in the current levels. Even though we applied voltages larger than the limti for electrochemical enlargement of the pores (> 0.75 V)[16], there was no change in the behavior in time suggesting that the exposed pore area is not due to MoS_2. The nonlinearity of the curve matches the models for gas bubble temporary electrowetting by Smirnov et al.[17]. We interpret this as a wetting issue (air bubble) over he membrane due to the use of alcohol prewetting, which the original MoS_2 membrane possibly damaged.

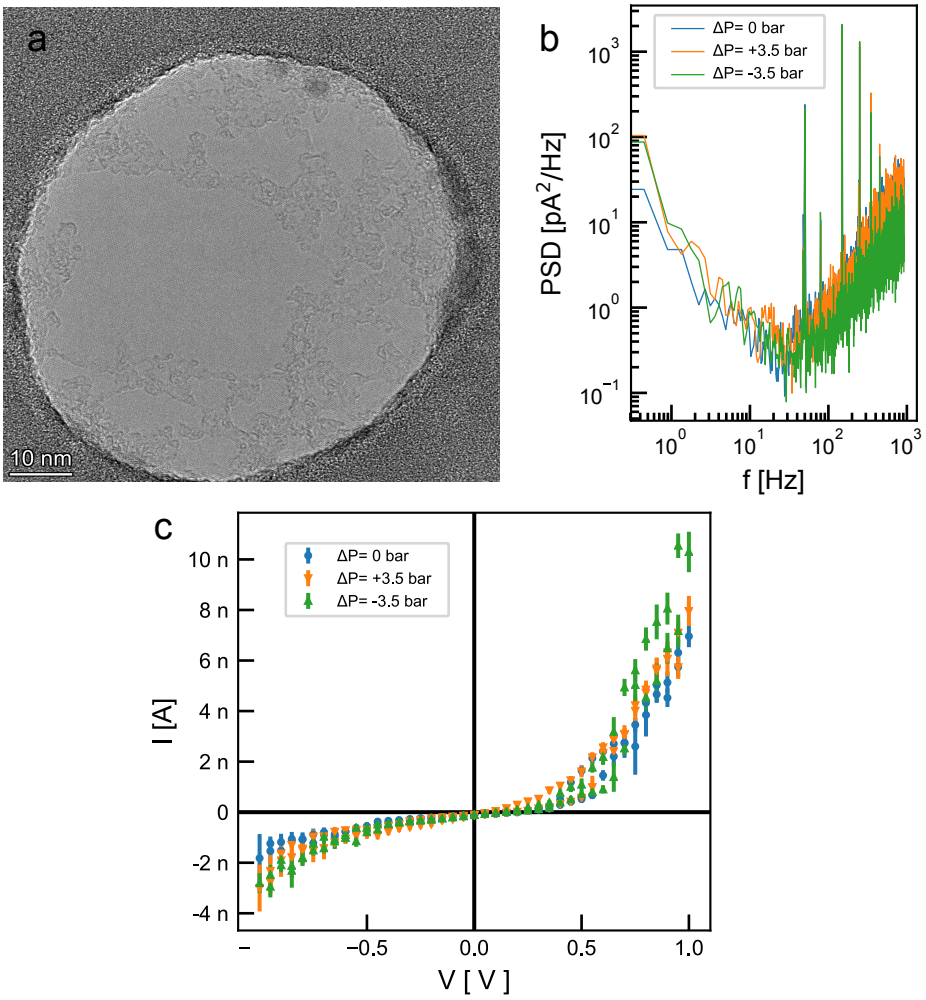

FIG. S10: **Sample $S_{MoS_2}3$** a) Transmission electron microscope images of MoS_2 sample before measurements. Imaged with FEI TEM Talos at 80 kV in HRTEM mode. b) IV curve of the sample IV curves after alcohol prewetting and then flushed with degassed solution. c) Noise power spectral densities (at +0.2 V). Both panel b and c are given under three different pressure gradients $\Delta P = 0, 3.5, -3.5$ bar showing no significant pressure dependence. Further application of compression pressure and flushing degassed solution did not change the state of the system until the membrane broke. The IV curve in the range of ± 0.5 V would indicate a nanopore in the ~ 1 nm range. We interpret this as being a wetting issue due to the alcohol prewetting.

Sample $S_{MoS_2}4$: The membrane was filled with degassed 1M KCl buffered at pH8 as described in the main text. After the application of 7 bar compression pressure for several minutes. First measurements indicated a high resistive IV curve (Fig. S11a) which was fluctuating between levels indicating current levels comparable to just the supporting membrane with no MoS_2 present (Fig. S11b). We conclude there are wetting issues due to the presence of gas bubbles and possible other contaminants. Application of pressure gradients and compression pressure (Fig. S11c) indicate that under compression the resistance of the pore is stable and high, but that gradient pressure moves the pore between low and high resistances, with the low resistance state indicating a low level of ionic current rectification indicating

better wetting.

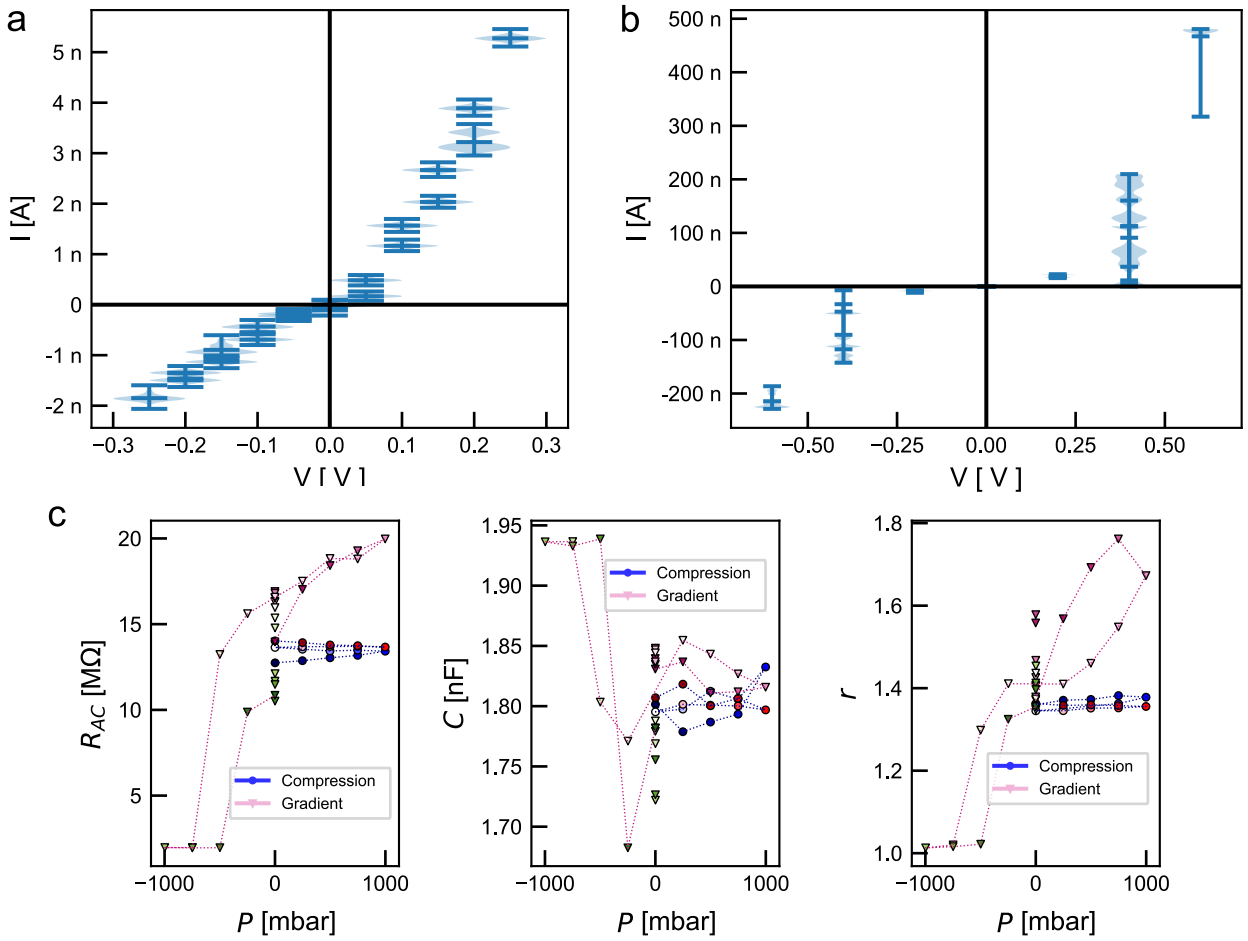

FIG. S11: **Sample $S_{MoS_2}4$**: a) Immediately after filling of the chamber. The bars indicate extrema and the mean value while the shape of the curve represents the current probability density (violin plot). The system stayed in this state for an hour or more without any noticeable change in the noise spectrum. b) Testing the sample with voltages up to 0.7 V a day after panel a. The bars indicate extrema and the mean value while the shape of the curve represents the current probability density (violin plot). The voltage was not varied in a regular way as in all other IV curves. Note that the applied voltages in this stage were below the reported voltages expected to cause an electrochemical reaction (0.75 V)[16]. Note the high level of current fluctuationss especially above 0.3 V. We attribute this to bubble or wetting/dewetting fluctuations. c) AC Pressure sweeps done after panel b. The first measurement is done using compression pressure and shows no change of the IV curves between two states, while in the gradient pressure the resistance changes between two states with a different state stable under no applied pressure. The lowest resistance state at $P < 0$ has no ionic current rectification.

Sample $S_{MoS_2}5$: The sample was imaged in TEM and drilled to have a pore of about $d =\approx 3-4$ nm with at least one smaller satellite pore (Fig. S12a). The pore was filled with degassed 1M KCl buffered at pH8 as described in the main text. After the application of 7 bar compression pressure, its current versus voltage characteristic was measured with the voltage always lower than the voltages known to cause electrochemical enlarging of the pores (< 0.75 V)[16]. Time evolution of the IV curves in the system indicated that the current levels were fluctuating between several states in time (Fig. S12b) with the most conductive state corresponding to roughly the expected pore resistance based on the TEM imaging. All these curves had the same level of Flicker noise. The sample was then flushed with freshly degassed solution and compression pressure was applied for several minutes. All the IV curves linearized and each further application of compression pressure was changing the pore resistance (Fig. S12c), with the high resistance state having the largest Flicker noise level (Fig. S12d. We believe this was a nanobubble pinned near the pore entrance (wetting issue) which was being slowly dissolved by applying compression pressure and a degassed solution. The original pore in MoS_2 possibly enlarged during handling (as it had at least one smaller satellite pore) or the membrane broke.

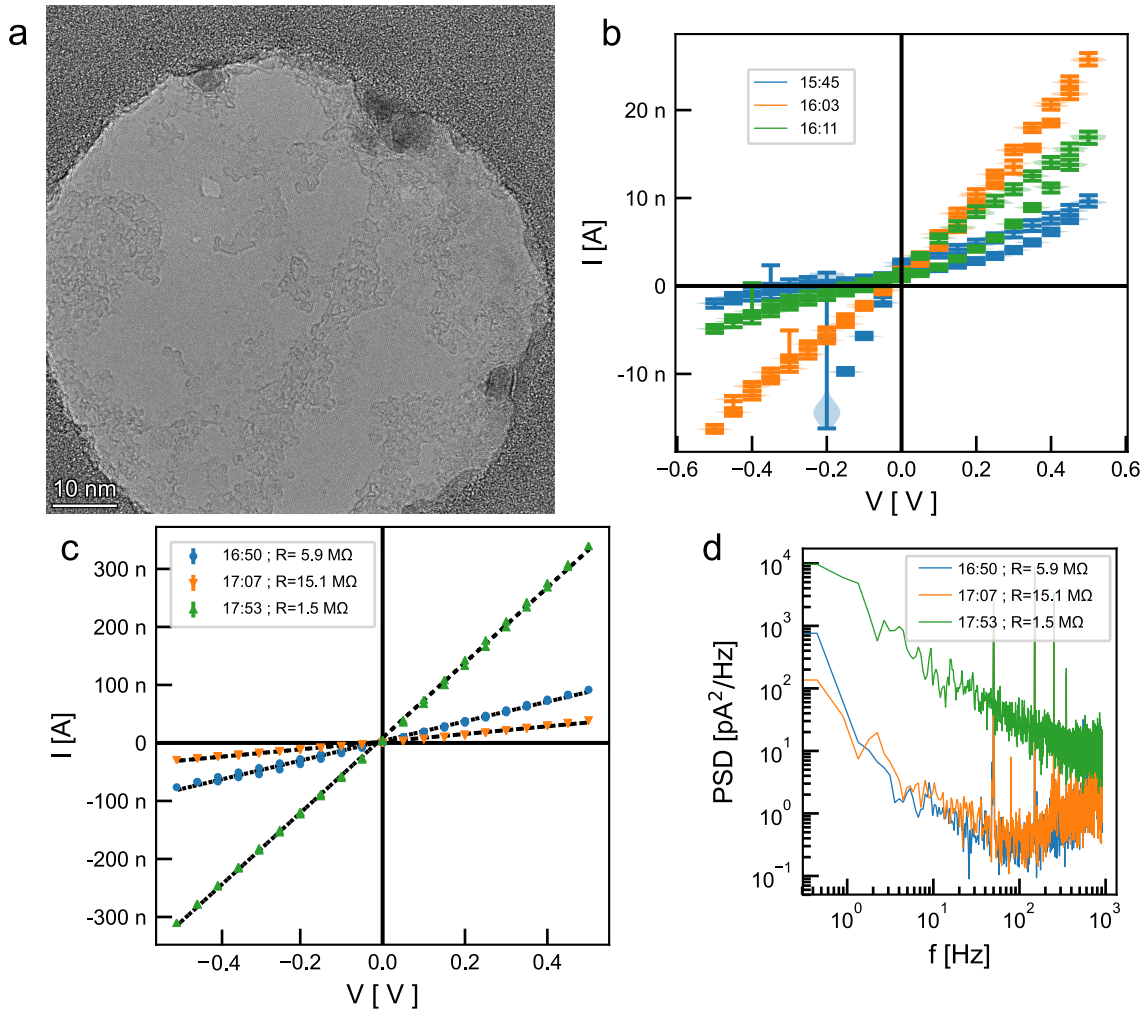

FIG. S12: **Sample $S_{MoS_2}5$**: a) Transmission electron microscope images of MoS_2 sample before measurements. Imaged with FEI TEM Talos at 80 kV in HRTEM mode. Visible nanopores were drilled by beam condensation with in-situ control of the pore formation. b) Three IV curves recorded about 10 minutes apart show fluctuations between a highly rectifying and almost linear IV curve. Power spectral densities of the ionic currents showed no significant difference in the flicker noise of the sample during this evolution. The most linear curve would correspond to a resistance of $R \approx 25$ MΩ, or to a MoS_2 pore of size $d \approx 4$ nm. Based on the drilled TEM image we would expect the pore to have a size of $d \approx 3 - 4$ nm.

[1] D. V. Verschueren, W. Yang, and C. Dekker, Nanotechnology **29** (2018), 10.1088/1361-6528/aaabce.
[2] V. Dimitrov, U. Mirsaidov, D. Wang, T. Sorsch, W. Mansfield, J. Miner, F. Klemens, R. Cirelli, S. Yemenicioglu, and G. Timp, Nanotechnology **21**, 065502 (2010).
[3] F. Traversi, C. Raillon, S. M. Benameur, K. Liu, S. Khlybov, M. Tosun, D. Krasnozhon, A. Kis, and A. Radenovic, Nat. Nanotechnol. **8**, 939 (2013).
[4] R. Karnik, C. Duan, K. Castelino, H. Daiguji, and A. Majumdar, Nano Lett. **7**, 547 (2007).
[5] S. W. Kowalczyk, A. Y. Grosberg, Y. Rabin, and C. Dekker, Nanotechnology **22**, 315101 (2011).
[6] J. Newman and K. E. Thomas-Alyea, *Electrochemical Systems*, 3rd ed. (2004).
[7] M. Takahashi, J. Phys. Chem. B **109**, 21858 (2005).
[8] M. Firnkes, D. Pedone, J. Knezevic, M. Doblinger, and U. Rant, Nano Lett. **10**, 2162 (2010).
[9] D. Lohse and X. Zhang, Rev. Mod. Phys. **87**, 981 (2015).
[10] N. Laohakunakorn, V. V. Thacker, M. Muthukumar, and U. F. Keyser, Nano Lett. **15**, 695 (2015).
[11] R. D. Bulushev, S. Marion, and A. Radenovic, Nano Lett. **15**, 7118 (2015).
[12] N. Laohakunakorn, B. Gollnick, F. Moreno-Herrero, D. G. A. L. Aarts, R. P. A. Dullens, S. Ghosal, and U. F. Keyser, Nano Lett. **13**, 5141 (2013).
[13] W.-J. Lan, D. A. Holden, and H. S. White, J. Am. Chem. Soc. **133**, 13300 (2011).
[14] L. Jubin, A. Poggioli, A. Siria, and L. Bocquet, Proc. Natl. Acad. Sci. **115**, 4063 (2018).
[15] P. Waduge, R. Hu, P. Bandarkar, H. Yamazaki, B. Cressiot, Q. Zhao, P. C. Whitford, and M. Wanunu, ACS Nano **11**, 5706 (2017).
[16] J. Feng, K. Liu, M. Graf, M. Lihter, R. D. Bulushev, D. Dumcenco, D. T. L. Alexander, D. Krasnozhon, T. Vuletic, A. Kis, and A. Radenovic, Nano Lett. **15**, 3431 (2015), arXiv:1504.04962.
[17] S. N. Smirnov, I. V. Vlassiouk, and N. V. Lavrik, ACS Nano **5**, 7453 (2011).